Laser-induced surface structuring for electron cloud mitigation in particle accelerators

Elena Bez[1,3], Marcel Himmerlich[1], Ana Karen Reascos Portilla[1], Lucie Baudin[1], Pierre Lorenz[2], Klaus Zimmer[2], Mauro Taborelli[1], André Anders[2]

[1]CERN, European Organization for Nuclear Research, 1211 Geneva 23, Switzerland

[2]Leibniz Institute of Surface Engineering (IOM), Permoserstr. 15, 04318 Leipzig, Germany

[3]University of Leipzig, Linnéstr. 5, 04103 Leipzig, Germany

Pulsed laser processing of vacuum component surfaces is a promising method for electron cloud mitigation in particle accelerators. By generating a hierarchically structured surface, the escape probability of secondary electrons is reduced. The choice of laser treatment parameters – such as laser power, scanning speed and line distance – has an influence on the resulting surface morphology as well as on its performance. The impact of processing parameters on the surface properties of copper is investigated by Secondary Electron Yield (SEY) measurements, Scanning Electron Microscopy (SEM), ablation depth measurements in an optical microscope and particle release analysis. Independent of the laser wavelength (532nm and 1064nm), it was found that the surface morphology changes when varying the processing parameters. The ablation depth increases and the SEY reduces with increasing laser fluence. The final application requires the capability to treat tens of meters of vacuum pipes. The limiting factors of this type of surface treatment for the applicability in particle accelerators are discussed.

1. Introduction

In particle accelerators, primary electrons are generated from proton beam induced residual gas ionization or photoemission due to synchrotron radiation. By interacting with the vacuum chamber walls, secondary electron multiplication can occur and lead to an electron cloud build-up that possibly induces a pressure rise, beam instabilities, heat loads to the cryogenic system of the beam pipe and surrounding superconducting magnets, and eventually a magnet quench [1,2].

To avoid electron multiplication, the secondary electron yield (SEY) of the surface facing the beam shall ideally be close to 1 or below. The SEY is the ratio of number of electrons emitted from the surface per incident electron. Pulsed laser processing is one possibility to reduce the SEY of a surface by generating grooves decorated with nano-size features that can trap secondary electrons [3-7]. However, the amount of ablated material must be optimized. First, the density of loose surface copper nanoparticles needs to be limited, since in an accelerator they could be released from the surface randomly, interact with the beam and provoke a beam dump due to emission of hard radiation or due to a magnet quench. Second, during treatment the ablated material can be deposited on the laser optics and degrade the quality of the process. In the case of the Large Hadron Collider (LHC), the thickness of the copper layer on the beam screen hosting the particle beam in vacuum amounts to 75 µm. The ablation depth of the generated grooves should not exceed 25 µm to keep the surface resistivity low and limit the heat load induced by the image current. The challenge for large-scale processing (tens of meters) is to achieve an acceptable scanning speed by keeping a sufficiently low SEY, limiting the ablation depth and reducing the amount of loosely bound particles on the surface. The present contribution deals with the optimization of the treatment parameters along the conceptional points mentioned above.

2. Experimental

Flat Oxygen Free Electronic (OFE) grade copper samples were degreased and chemically passivated beforehand. After cleaning, they were treated in air using a Nd:YVO_4 laser with a fixed pulse duration (12 ps) and repetition rate (f = 100 kHz). The primary (1064 nm) and the frequency doubled laser wavelength (532 nm), were employed. The beam is focussed onto the surface by a f-theta lens with focal length of 165 mm. The gaussian beam diameter ($1/e^2$) is 11.6 µm (green) and 26.4 µm (IR), respectively. The laser beam was scanned along parallel lines using a Galvano-scanner at line distances Δy of 10 µm and 50 µm. The scanning speed v was varied between 1 mm/s and 200 mm/s. The maximum time-averaged laser power P was 1.6 W (green) and 3.4 W (IR), respectively. This power was gradually attenuated for each laser wavelength. All the indicated fluences F in this report refer to the accumulated energy E per surface area and are calculated by the following equation:

$$F = (E/f)/v\Delta y = P/v\Delta y.$$

To observe and measure the grooves profile, the laser treated samples were mechanically ground on silicon carbide discs and polished afterwards using aluminium oxide abrasive. Once the cross-section is visible, the ablation depth is measured with an optical microscope. The given values always refer to the maximum depth measured from the untreated surface level to the valley

of the trenches as indicated in Figure 1a) by the dashed green lines.

Centrifugation tests on treated samples were carried out to estimate the amount of copper particles released from the surface by a well-defined acceleration. The samples were mounted into a centrifuge with the treated surface facing outward with respect to the rotational axis so that inertia forces (26 N/mm^3) act perpendicular to the macroscopic surface. The applied force of 26 N/mm^3 corresponds to the force acting on the beam screen in case of a magnet quench. The detached particles are detected by a carbon sticker placed in front of the sample surface and identified in SEM by Automatic Particle Analysis (APA) [8].

For SEY analysis, an electron beam of 2 nA was focused to a spot diameter of 1 mm on the sample surface and the primary electron energy was gradually increased from 50 to 1800 eV. The measurement was performed in two steps. First, the primary current was acquired by applying a positive voltage (+45 V) on the sample. Both primary (PE) and recaptured secondary electrons (SE) were measured on the sample. In the second step, the sample was negatively biased (-45 V) so that secondary electrons were repelled from the surface. The secondary electron current was determined to $I_{SE} = I_{PE} - I_{sample}$. Consequently, the SEY δ in dependence of the electron energy was calculated by:

$$\delta(E) = I_{SE}(E)/I_{PE}(E).$$

A detailed description of the SEY setup is described in Ref. [9].

3. Results and Discussion

The analysis was focused on the limiting factors for the application in particle accelerators, namely the ablation depth, the SEY**,** the corresponding morphology and particle release from the surface.

3.1. Surface topography

The surfaces generated in this work are macroscopically roughened and are of black appearance. They exhibit characteristics on the micro- and nanoscale which are visible in Figure 1. Along the laser scanning direction, trenches are created at the surface due to material ablation. Examples of cross-sections and top view scanning electron micrographs are depicted in Figure 1 (left and middle column). The distance between each valley corresponds to the line distance (*Δy* = 50 µm in this case). Additionally, the trenches are covered by nanoparticles originating from the redeposition of ablated material. The morphology depends drastically on the used laser parameters. When reducing the scanning speed, the groove depth expectedly increases. Moreover, the nanostructure exhibits different shapes. At a scanning speed of 1 mm/s, compact cauliflower shapes are formed, whereas at higher scanning speeds, less material is ablated and consequently only few redeposited particles as well as molten and resolidified spheres cover the surface. The SEM image in Figure 1c) of a sample processed at 20 mm/s depicts surface ripples that remind of Laser Induced Periodic Surface Structures (LIPSS) [10].

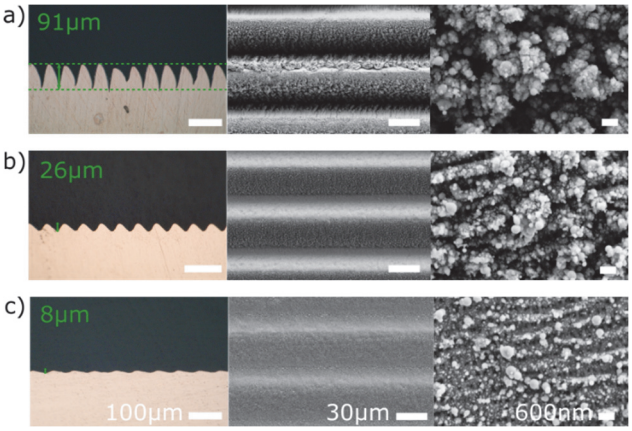

Figure 1: Micro- and nanostructures of 532 nm laser irradiated copper at constant time-averaged laser power of P = 1.64 W and line distance *Δy* = 50 µm. Varied scanning speed of a) v = 1 mm/s (F = 3280 J/cm²), b) v = 5 mm/s (F = 656 J/cm²) and c) v = 20 mm/s (F = 164 J/cm²). The scale bars refer to 100 µm for the microscope images in the left column, as well as 30 µm and 600 nm for the SEM images in the middle and right column, respectively.

3.2. Ablation depth

The ablation depth was measured for employed wavelengths of 532 nm and 1064 nm on samples for which the laser power and the scanning speed were varied during processing. The ablation depth as a function of accumulated fluence is presented in Figure 2 on a double logarithmic scale. For the two wavelengths, the ablation depth increases monotonically. The data points diverge slightly at depths of only a few micrometres, which can be explained by the resolution limit of the optical microscope.

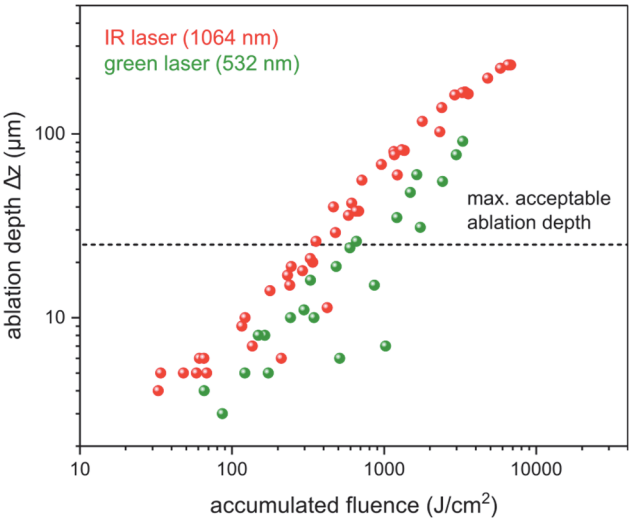

Figure 2: Ablation depth for 1064 nm and 532 nm laser irradiation as a function of accumulated fluence at a fixed line distance of 50 µm.

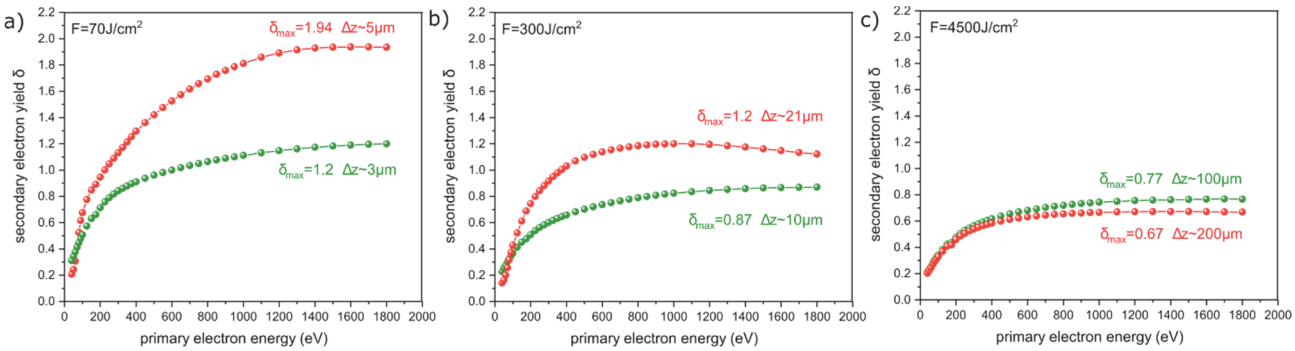

Figure 3: Secondary electron yield in dependence of primary electron energy for 1064 nm (red dots) and 532 nm (green dots) as a function of laser fluence F and corresponding ablations depths Δz.

At similar fluences, infrared laser irradiation results in deeper grooves compared to the green laser. Since the IR gaussian diameter is twice the size of the green laser diameter, the ablated volume per pulse is accordingly higher. The IR laser seems more effective even if the reflectivity of copper at λ = 532 nm is lower than at λ = 1064 nm [11]. The reason may be that after the first few pulses, the surface starts to roughen, and the initial reflectivity drops. At higher laser power, not only linear, but also non-linear absorption of the laser light by the material as well as by the gas phase of expanding particles play a role. Particularly at low scanning speeds, plasma shielding effects cannot be excluded. For the final application, the maximum ablation depth should ideally be less than 25 µm to keep the surface resistivity low.

3.3. Secondary Electron Yield

By generating rough surfaces, electrons are trapped by the fissured topography and consequently the SEY is reduced [12]. Figure 3 depicts the SEY in dependence of the primary electron energy (50 – 1800 eV) for λ = 532 nm and λ = 1064 nm. The accumulated fluence F increases from left to right. In all cases, the SEY maximum was reduced from δ_{max} ~ 2.2 of a degreased copper surface [8,13]. The lowest achieved δ_{max} accounts to 0.67. It is evident, that the SEY maximum decreases with accumulated fluence for both wavelengths. Furthermore, the differences in SEY curves between the two laser wavelengths decrease accordingly. The green laser seems to be more beneficial regarding SEY reduction, especially in the low fluence range (Figure 3a). As demonstrated in Figure 3c), similar SEY curves are obtained at sufficiently high fluences. Linking the morphology to the shown SEY curves, the cauliflower shapes correspond to δ_{max} ~ 0.7, whereas the ripple structures, decorated with diverse particles, exhibit a maximum SEY of δ_{max} ~1.2.

3.4. Particle analysis

After centrifugation of 532 nm laser treated samples, an increase of ~0.1 in SEY maximum is observed. Figure 4 presents the corresponding SEY curves. The SEY increase is caused by the detachment of nanoparticles that cover the surface. The size distribution of particles released per surface area is presented in Figure 5. On average, the particle diameter accounts to 4 µm. The global number density of detected particles is roughly about 18000 per cm^2. Further details of the investigations on particle release are described in Ref. [8].

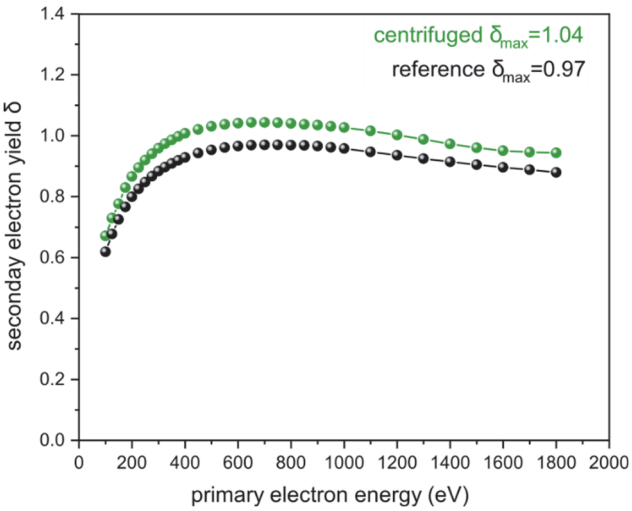

Figure 4: SEY of 532 nm laser treated copper before (reference) and after centrifugation at an inertial force of 26 N/mm^3 and an accumulated fluence of F = 593 J/cm^2.

In the final application, tens of meters of vacuum pipes need to be treated. Therefore, the process must be scaled up and the treatment speed must be increased. Especially, a laser–glass fibre coupling system and other optical components are required to guide the light towards the reaction zone. These adaptions will lead to a lower fluence accumulated on the surface and one must consider that the SEY will increase according to Figure 3. The advantage would be that the processing at lower fluence results in shallower grooves that are covered with only a few redeposited nanoparticles or molten and resolidified spheres (Figure 1). Moreover, the aimed SEY maximum of 1 can still be reached without exceeding the maximum ablation depth of 25 µm. According to the investigations, the SEY maximum of unity is reached at an accumulated fluence of 130 J/cm^2 for the green and 650 J/cm^2 for the IR laser, respectively. Thus, one would need 4 days (using a green laser) and 20 days using an IR laser to treat a 10 m beam screen of a dipole, assuming a laser power of 5 W and a line distance of 50 µm. However, in contrast to a green laser system, coupling of

picosecond pulsed IR laser light into a glass fibre allows operation at average output powers higher than 5 W.

The choice of laser wavelength has an influence on the ablation efficiency as well as on the SEY. Particularly at low fluences, the SEY is rather high when utilising an IR laser. Nevertheless, for IR lasers exist more technological solutions for guiding the laser light to the internal surface of a beam pipe compared to green lasers.

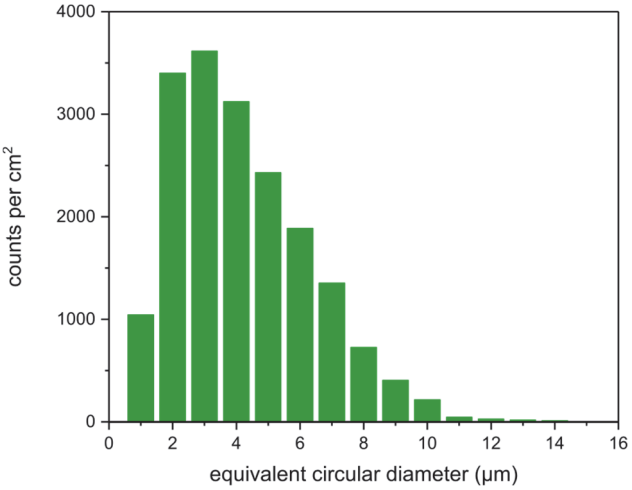

Figure 5: Size distribution of released particles after centrifugation at an inertial force of 26 N/mm^3 of a laser treated sample (λ = 532 nm, F = 593 J/cm2).

4. Conclusions

The present study defines the range of parameters to perform a suitable surface treatment for SEY reduction respecting the requirements for a particle accelerator. At rather low fluences, a sufficiently low SEY maximum is reached within the constraints of the ablation depth. As only few particles are generated at such low fluences, the detachment of particles will most likely play a minor role. All this is the base to enable the integration of such laser processing in the treatment of the complex geometry of a long pipe. From the results obtained so far, both wavelengths (green and infrared) could meet the requirements for SEY reduction and ablation depth minimization. The choice will depend on the further conditions for the integration of the treatment in the real geometry of a vacuum pipe and on the commercial availability of optical components.

Acknowledgements

The authors thank Karolina Bogdanowicz, Aidan Gunn and Stephan Pfeiffer (CERN EN-MME-MM) for cross-section preparation and microscopy analysis. The support by the Wolfgang Gentner Programme of the German Federal Ministry of Education and Research (grant no. 05E18CHA) for the PhD studies of Elena Bez are gratefully acknowledged.

References

[1] R. Cimino, T Demma, International Journal of Modern Physics A, 29 (2014), 1430023.

[2] G. Rumolo, F. Ruggiero, F. Zimmermann, Physical Review Special Topics - Accelerators and Beams, 4 (2001), 012801.

[3] R. Valizadeh, O. B. Malyshev, S. Wang, S. A. Zolotovskaya, W. A. Gillespie, A. Abdolvand, Applied Physics Letters, 105 (2014), 231605.

[4] R. Valizadeh, O. B. Malyshev, S. Wang, T. Sian, M. D. Cropper, N. Syke, Applied Surface Science, 404 (2017), 370 – 379.

[5] S. Calatroni, E. Garcia-Tabares Valdivieso, H. Neupert, V. Nistor, A. T. Perez Fontenla, M. Taborelli, P. Chiggiato, O. Malyshev, R. Valizadeh, S. Wackerow, S. A. Zolotovskaya, W. A. Gillespie, A. Abdolvand, Physical Review Accelerators and Beams, 20 (2017), 113201.

[6] S. Calatroni, E. Garcia-Tabares Valdivieso, A. T. Perez Fontenla, M. Taborelli, H. Neupert, M. Himmerlich, P. Chiggiato, D. Bajek, S. Wackerow, A. Abdolvand , Physical Review Accelerators and Beams, 23 (2020), 033101.

[7] D. Bajek., S. Wackerow, D. A. Zanin, L. Baudin, K. Bogdanowicz, E. Garcia-Tabares. Valdivieso, S. Calatroni, B. Di Girolamo, M. Sitko, M. Himmerlich, M. Taborelli, P. Chiggiato, A. Abdolvand, Scientific Reports, 10 (2020), 250.

[8] L. Baudin, PhD Thesis, Université Paris Sciences et Lettres, 2020, 2020UPSLM052, http://www.theses.fr/2020UPSLM052.

[9] V. Petit, M. Taborelli, D. A. Zanin, H. Neupert, P. Chiggiato, M. Belhaj, Physical Review Accelerators and Beams, 23 (2020), 093101.

[10] J.J.J. Nivas, M. Valadanb, M.Salvatore, R. Fittipaldi, M. Himmerlich, M.Rimoldi, A.Passarelli, E. Allahyar, S.L.Oscurato, A.Vecchione, C.Altucci, S.Amoruso, A. Andreone, S. Calatroni, M. R. Masullo, Surfaces and Interfaces, 25 (2021), 101179.

[11] P. B. Johnson, R. W. Christy, Physical Review. B, 6 (1972), 4370-4379.

[12] M. Pivi, F. K. King, R. E. Kirby, T. O. Raubenheimer, G. Stupakov, F. Le Pimpec, Journal of Applied Physics, 104 (2008), 104904.

[13] R. Cimino, L. A. Gonzalez, R. Larciprete, A. Di Gaspare, G. Iadarola, G. Rumolo, Physical Review Special Topics - Accelerators and Beams, 18 (2015), 051002.